

The Deconfinement Transition in $SO(3)$ Gauge Theory

Saumen Datta¹ and R.V. Gavai²

*Theoretical Physics Group,
Tata Institute of Fundamental Research,
Homi Bhabha Road, Mumbai 400005, India*

Abstract

The $SO(3)$ lattice gauge theory with a Villain form of action was investigated by Monte Carlo techniques on asymmetric lattices with $N_\tau = 2$ and 4, where N_τ is the number of sites in the temporal extent. Unlike the results for higher N_τ , only one transition of second order was found for $N_\tau = 2$. An extended action with an irrelevant term to suppress Z_2 monopoles enabled us to get a better view of the deconfinement transition as the effects of bulk transition could be suppressed as well. Although the action has no global Z_2 -symmetry for the $SO(3)$ theory, unlike the $SU(2)$ theory at finite temperature, our study revealed a second order deconfinement transition, with properties similar to the deconfinement transition of $SU(2)$.

PACS code: 11.15.Ha,12.38.Aw

Keywords: Deconfinement, $SO(3)$ Gauge Theory, Z_2 -monopoles.

¹E-mail:saumen@theory.tifr.res.in

²E-mail:gavai@theory.tifr.res.in

1 INTRODUCTION

The most convenient way of regularizing gauge theories for nonperturbative studies is by discretizing the underlying space-time on a lattice. The gauge variables can then be chosen as suitable representations of the gauge group residing on the links of the lattice.

A natural choice for the lattice action is the Wilson action [1], in which the gauge variables are in the fundamental representation of the gauge group. For the SU(2) gauge theory, the action is simply

$$S_W = \frac{\beta_f}{2} \sum_p \text{Tr}_f(U_p) \quad (1)$$

where U_p is the product of link variables around a plaquette, and the subscript f denotes the trace is to be taken in the fundamental representation of the gauge group. The fundamental representation is particularly convenient when one includes fermions, since the fermions are normally taken in this representation. The Wilson action has been widely studied in the literature, both for zero-temperature and finite temperature studies. Studies of gauge theories at finite temperature can be performed by taking a lattice with a finite temporal extent equal to the inverse temperature, and imposing periodic boundary conditions on the gauge variables in the temporal direction. One interesting prediction that has emerged from such studies is that, at a sufficiently high temperature, the theory undergoes a deconfinement transition. The finite temperature gauge theory has a global symmetry corresponding to the center of the gauge group. The deconfinement transition is generally described by the breaking of this center symmetry. The Polyakov loop operator,

$$L_f(\vec{r}) = \text{Tr}_f \prod_{i=1}^{N_\tau} U_\tau(\vec{r}, i), \quad (2)$$

transforms non-trivially under this symmetry and therefore acts as an order parameter for the deconfinement transition. Here N_τ is the number of lattice points in the temporal direction.

The Wilson action (1) is by no means the only choice for the discretized action. Since the continuum theory is at a critical point of the lattice regularized theory, one expects a large class of actions, differing only by irrelevant terms, to correspond to the same continuum physics. In particular, one can

take the trace in (1) in any representation of the gauge group. Since the continuum theory is defined only in terms of the underlying algebra, the choice of the representation for the link variables should be completely irrelevant for it.

One particularly interesting variant of (1) is when the trace is taken in the adjoint representation. The gauge variables in adjoint representation are blind to the center of the group. The center symmetry is therefore absent and $\langle L_f \rangle$ is identically zero. A study of the deconfinement transition for this form of the action is therefore of particular interest [2].

Finite temperature $SO(3)$ gauge theory was studied in refs. [3, 4] with the Wilson form for the action, and in ref. [5] using a Villain form [6]. A natural analog of $\langle L_f \rangle$ was taken to be $\langle L_a \rangle$ where the adjoint Polyakov loop L_a is defined as

$$L_a(\vec{r}) = \text{Tr}_a \prod_{i=1}^{N_\tau} U_\tau(\vec{r}, i). \quad (3)$$

While $\langle L_a \rangle$ is not an order parameter for the deconfinement transition as the screening of an adjoint quark renders it to be non-zero in the confined phase, it is known to behave quite similarly as $\langle L_f \rangle$ across the $SU(2)$ deconfinement transition. It was found in refs.[3, 4, 5] that the finite temperature theory shows a discontinuous transition. $\langle L_a \rangle \simeq 0$ till the transition point, where it rises sharply, indicating a deconfining nature of the transition. The transition point, however, was coincident with the known bulk transition point for $SO(3)$ [7]. Moreover, it did not shift with increasing temporal extent of the lattice [4, 5], which is both unlike the deconfinement transition in the $SU(2)$ theory and characteristic of a bulk transition.

These results appear to be similar to those obtained in refs. [8, 9] in finite temperature studies with the Bhanot-Creutz action [7]

$$S = \sum_p \left[\beta_f \left(1 - \frac{1}{N} \text{Tr}_f U_p \right) + \beta_a \left(1 - \frac{1}{3} \text{Tr}_a U_p \right) \right]. \quad (4)$$

There too, a first order deconfinement line, as characterized by the order parameter $\langle L_f \rangle$, was found to be coincident with the previously known first order bulk transition line for a range of large β_a . Moreover, the shift in the transition coupling with changing N_τ was found to be negligibly small although it increased progressively as β_a was decreased.

Both for the intrinsic importance of the study of the deconfinement transition for the $SO(3)$ gauge theory, and in order to have a better understanding

of the interplay between the bulk and deconfinement transitions, we thought it necessary to conduct further detailed studies of the $SO(3)$ gauge theory at finite temperature. To decouple the two transitions, we 1) employed $N_\tau = 2$ lattices in our simulations (a sizeable shift in the transition point was seen for $N_\tau = 2$ lattices in ref. [9] for the Bhanot-Creutz action) and 2) have used extended actions [10] to suppress the bulk transition so as to get a clearer view of the deconfinement transition. As in ref. [5], we have used the Villain form of the $SO(3)$ action. The plan of our paper is as follows: in Sec. 2, we present results for the phase transition for the $N_\tau = 2$ and 4 lattices. In Sec. 3, the phase transition for the extended action is discussed. The last section contains a summary of our results and their discussion.

2 PHASE TRANSITION FOR THE VILLAIN ACTION

2.1 The Action and its Properties

In the Villain form of the action for the $SO(3)$ theory from ref. [6], one introduces auxiliary Z_2 variables σ_p associated with the elementary plaquettes, besides the usual gauge variables in the fundamental representation of the gauge group $SU(2)$. The $SO(3)$ theory is defined by the partition function

$$Z = \sum_{\{\sigma_p = \pm 1\}} \int \mathcal{D}U \exp(S(U, \sigma)) \quad (5)$$

where the action S is given by

$$S(U, \sigma) = \frac{\beta_v}{2} \sum_p \text{Tr}_f(U_p) \cdot \sigma_p. \quad (6)$$

On performing the summation over the σ_p variables, one gets the gauge field effective action

$$S_{\text{eff}}(U) = \sum_p \ln \cosh \left(\frac{\beta_v}{2} \text{Tr}_f U_p \right) \quad (7)$$

which is clearly blind to the center symmetry. The character expansion of $e^{S_{\text{eff}}}$ has contributions only from the integer representations of $SU(2)$ [10]. Explicitly, the link variables have the local Z_2 symmetry

$$U_l \rightarrow -U_l, \quad \sigma_p \rightarrow -\sigma_p \quad \forall p \ni \hat{\partial}l. \quad (8)$$

The connection to the $SU(2)$ gauge theory with Wilson action in the weak coupling limit is clear: as $\beta_v \rightarrow \infty$, the configurations that contribute are

$$U_l = \sigma_l e^{igA}, \quad \sigma_p = \prod_{l \in \partial p} \sigma_l \quad (9)$$

where σ_l are Z_2 variables situated on the links. Then a change of variable $U_l \rightarrow U_l \sigma_l$ reproduces the $SU(2)$ gauge theory with Wilson action.

The theory (5) is known to have a bulk transition at $\beta_v \sim 4.45$ [6, 5]. This bulk transition has been explained by the condensate of Z_2 monopoles [6]. The two phases differ in the value of the monopole density, defined by [10]

$$M = 1 - \left\langle \frac{1}{N_c} \sum_c \sigma_c \right\rangle, \quad (10)$$

$$\sigma_c = \prod_{p \in \partial c} \sigma_p \quad (11)$$

where c denote the elementary cubes in the lattice and N_c is the number of such cubes. In the strong coupling phase,

$$M = 1 - 4\beta_{\frac{6}{2}}$$

where the character expansion coefficients β_j are given by

$$\beta_j = \frac{I_{2j+1}(\beta_v)}{I_1(\beta_v)}, \quad (12)$$

whereas in the weak coupling region, $M = 0$ up to exponential corrections. At the bulk phase transition point, M jumps from its strong coupling value to the weak coupling value.

2.2 Phase Transition at Finite Temperature

Numerical investigations of the finite temperature transition for this theory have been carried out in ref.[5]. By monitoring the plaquette variable, $P = \sigma_p \text{Tr}_f(U_p)$, and $\langle L_a \rangle$ (Eq. (3)), for lattices with N_τ ranging from 4 to 8, it was found that the theory has only one, strong first order, transition. The transition point was found to be $\beta_v \sim 4.45$ for all the lattices, with no perceptible change in β_{vc} . While this is typical of a bulk transition, the

Table 1: Free energy difference for Lee-Kosterlitz analysis.

N_σ	6	8	10	12	16	24
ΔF	.38(2)	.52(2)	.55(2)	.48(3)	.58(5)	.57(10)

behavior of $\langle L_a \rangle$ was indicative of a deconfining nature of the transition : it jumped across the transition, being $\simeq 0$ before the transition. One possible way to explain the curious mixture of the bulk and deconfining characteristics of the transition is to hypothesize a shielding of the deconfinement transition by a sufficiently strong first order bulk transition. However, since the deconfinement transition point is expected to shift with a change in N_τ , such a shielding will only be possible over a finite range of N_τ ; outside that range the two transitions have to separate out. Such a separation was not seen in ref. [5] for $N_\tau = 4$ to 8. Guided by the results of ref. [9], here we study $N_\tau = 2$ to explore the lower end of the range, as the shift in the deconfinement transition point is expected to be larger in going from $N_\tau = 4$ to 2.

The transition point was indeed found to shift to $\beta_v \sim 4.16$ for $N_\tau = 2$. The nature of the transition, on the other hand, was found to be different. While a two-peak structure was found at the critical point, it did not sharpen with an increase in the spatial size of the lattice. We carried numerical simulations for lattices with spatial size $N_\sigma = 6, 8, 10, 12, 16$ and 24 (details of the simulation are given in Appendix A). Figure 1 shows the distribution of the plaquette and L_a for these lattices at β_{vc} . A two-peak structure is visible in all of them. However, the peaks move closer to each other as N_σ increases and the valley in between them becomes shallower. This is, of course, opposite to what one expects for a first order transition, and suggests either a second order transition or a crossover in the thermodynamic limit. From Fig. 1 one can calculate the free energy difference between the maxima and the minima for a given spatial volume, by using the spectral density method [11] to extrapolate the histograms to a β -value such that the two peaks are of equal height. For a first order transition, this difference ΔF is expected to increase with lattice size, while a plateau should be reached for a second order transition [12]. The estimates of ΔF , shown in table 1, clearly rule out a first order transition.

Further insight into the nature of the transition can be gained by looking

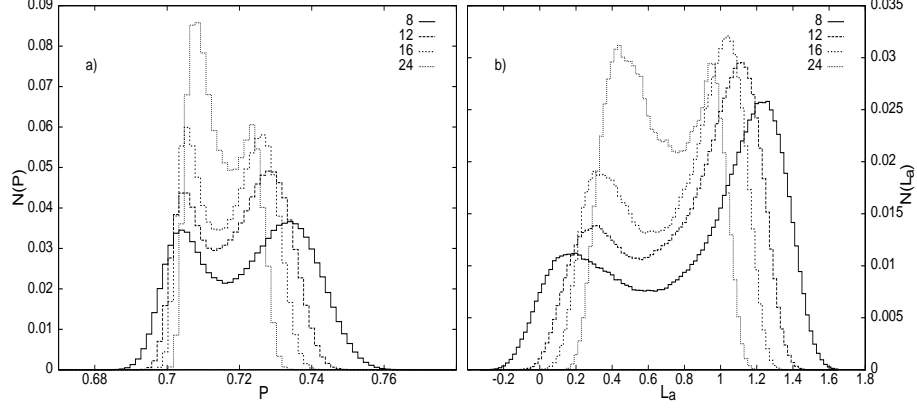


Figure 1: Distribution of a) plaquette and b) L_a for $N_\sigma^3 \times 2$ lattices with $N_\sigma = 8, 12, 16, 24$.

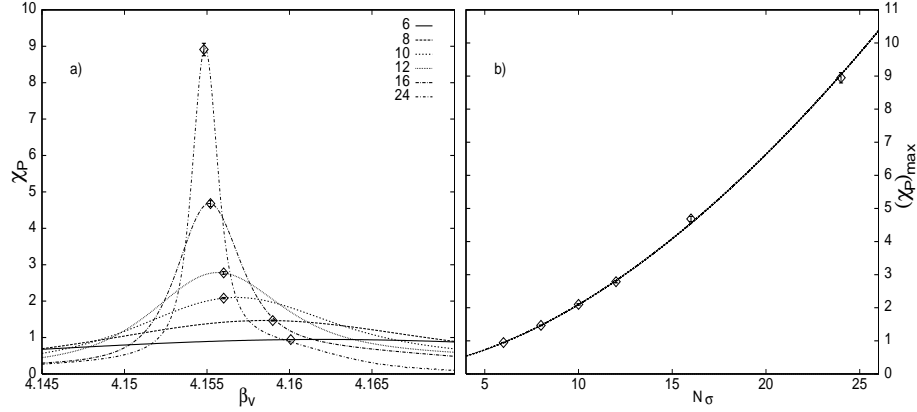


Figure 2: a) The plaquette susceptibility, Eq.(13), as a function of β_v for $N_\sigma = 6, 8, 10, 12, 16$ and 24 . The points show the couplings where runs were made for each lattice; the lines are Ferrenberg-Swendsen extrapolation. b) Peak of the plaquette susceptibility plotted against N_σ . Also shown is the best power law fit, discussed in the text.

Table 2: Fit parameters

	a	b	ω	$\frac{\chi^2}{d.f.}$
χ_P	$.14 \pm .07$	$(3.6_{-.7}^{+.8}) \times 10^{-2}$	$1.73 \pm .07$	1.12
χ_{L_a}	$-3.6 \pm .6$	$2.9_{-.5}^{+.6}$	$1.78 \pm .07$.69

at the plaquette- and L_a -susceptibilities

$$\chi_P = 12N_\sigma^3(\langle P^2 \rangle - \langle P \rangle^2), \quad (13)$$

$$\chi_{L_a} = N_\sigma^3(\langle L_a^2 \rangle - \langle L_a \rangle^2). \quad (14)$$

For a first order bulk transition, the plaquette susceptibility is expected to scale as the volume of the lattice [13]. Therefore, for our $N_\tau = 2$ lattices, they are supposed to scale as N_σ^3 . The peak heights are plotted against N_σ in Fig. 2 b). Also shown is the best fit to a form $\chi_{P_{max}}(N_\sigma) = a + b N_\sigma^\omega$. The corresponding values of the parameters are tabulated in table 2. The exponent is clearly different from the expectations for first order transition.

In case of a deconfinement transition, the peak of the L_a susceptibility may be expected to scale as N_σ^3 for a first order transition, and as N_σ^ω with $\omega \sim 1.97$ for an Ising-like transition. In Fig. 3 b) the peak heights are shown as a function of N_σ . The best fit to the form $a + b N_\sigma^\omega$ is also shown. It yields $\omega = 1.78 \pm 0.07$ which, amusingly, is not too far from expectations for an Ising-like transition.

The above behavior is in contrast to what is seen for $N_\tau = 4, 6$ and 8 lattices, where a strong first order transition was seen in ref. [5]. In fact, Fig. 1 is to be contrasted with Figs. 6 and 7 of ref. [5] for $N_\tau = 4$, where the peak positions remained stationary and the peak structure became sharper with increase in N_σ over the range 4 to 8. We have checked that the behavior does not alter on increasing the spatial lattice size by making fresh simulations for $N_\sigma = 16$ and 24 for $N_\tau = 4$. The resulting histograms are shown in Fig. 4, along with the $8^3 \times 4$ data from ref. [5]. They clearly indicate a first order transition for $N_\tau = 4$ lattices in the infinite volume limit, with discontinuities in plaquette and adjoint Polyakov loop given by, $\Delta P = .058 \pm 3, \Delta L_a = 0.87 \pm 0.04$.

The second order transition for the $N_\tau = 2$ case, with an exponent close to the 3-D Ising model, may prompt one to identify the transition with the

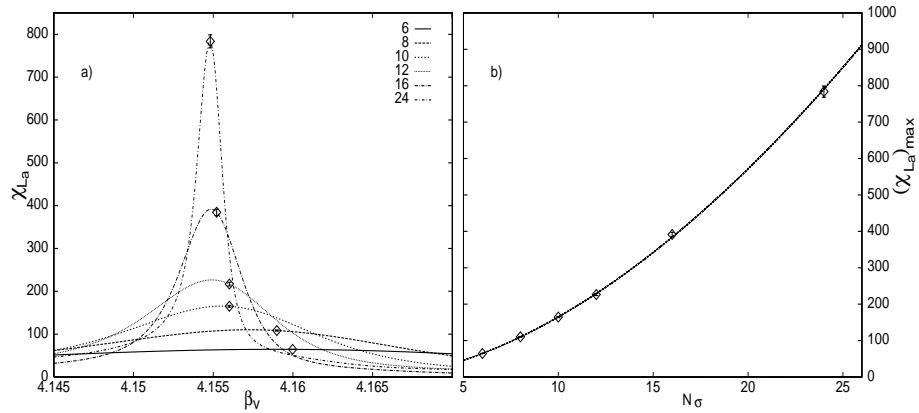


Figure 3: a) The Polyakov loop susceptibility, Eq.(14), as a function of β_v for $N_\sigma = 6, 8, 10, 12, 16$ and 24 . b) Peak of the Polyakov loop susceptibility plotted against N_σ . Also shown is the best fit discussed in text.

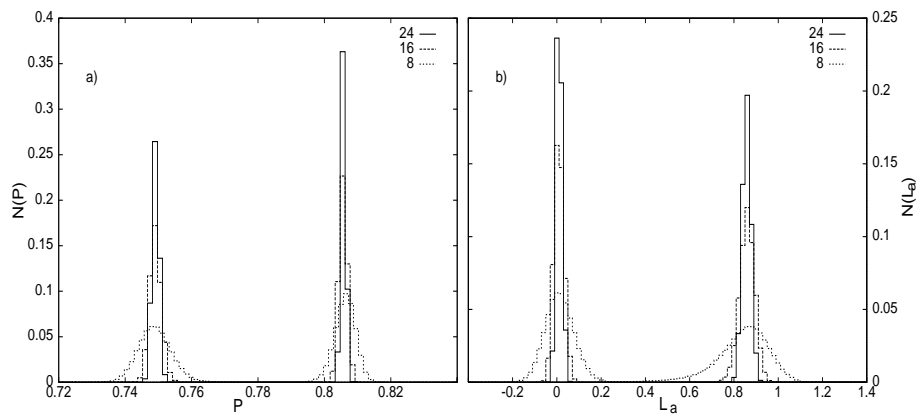


Figure 4: Distribution of a) plaquette and b) L_a for $N_\sigma^3 \times 4$ lattices with $N_\sigma = 8, 16, 24$.

$SU(2)$ deconfinement transition, thereby vindicating the shielding scenario above. However, on a closer examination, one sees that the detailed properties of the transition are very different from the $SU(2)$ case. The plaquette variable is smooth at the $SU(2)$ deconfinement transition point, and χ_{L_a} does not show criticality there [14], whereas from table 2 one finds that both χ_{L_a} and χ_P diverge at the $SO(3)$ transition with essentially the same exponent. This indicates that here too one is seeing an intricate interplay of bulk and deconfinement transition effects, very much like the higher N_τ cases. We believe that the reason the order of the transition changes in going from higher N_τ to $N_\tau = 2$ may simply be the fact that the latter have effectively a smaller bulk-dimensionality. This interpretation, suggested by the near equality of the exponents for χ_{L_a} and χ_P , indicates a more complicated interplay of the bulk and deconfinement transitions than the simple shielding scenario since a shielding is easy to justify only in the vicinity of a strong first order transition, while the $N_\tau = 2$ lattices show a mixing of effects of bulk and deconfinement transitions even in the presence of a continuous bulk transition. Moreover, it also calls for a different approach to disentangle the bulk effects from the deconfining ones. In the next section, we present results from an attempt in that direction.

3 PHASE TRANSITION FOR EXTENDED ACTION

Since the $SO(3)$ bulk transition is known to be caused by a condensation of Z_2 monopoles, which are purely topological lattice artifacts and do not survive in the continuum limit, one may hope to get a clearer view of the physics of the deconfinement transition in the $SO(3)$ theory by suppressing them, without missing any important continuum physics. One may be able to address important physics questions associated with the deconfinement transition in this manner, specially since there is no obvious order parameter in this case. The suppression can be achieved smoothly by adding a term to the action which disfavors the monopole configurations. The most obvious choice is to add a monopole chemical potential term to the action [10], as considered below.

3.1 Action and its properties

We study the action [10]

$$S_M(U, \sigma) = \frac{\beta_v}{2} \sum_p \text{Tr}_f(U_p) \cdot \sigma_p + \lambda \sum_c \sigma_c \quad , \quad (15)$$

where σ_c is defined in Eq. (11).

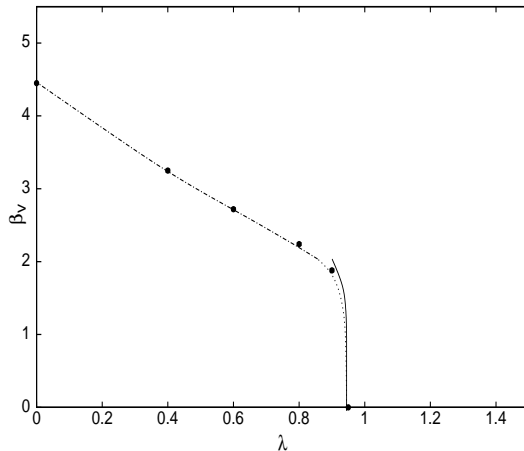


Figure 5: The phase diagram for action (15). The dotted line denotes a second order transition while the dot-dashed line denotes a first order line. The points are the actual simulation points. The full line is the approximation of Eq. (16).

This action has a line of phase transitions in the (β_v, λ) plane [10]. For $\lambda = 0$, it reduces to the action of Eq. (6), with a first order transition at $\beta_{vc} \sim 4.5$. For $\beta_v = 0$, the theory is dual to four dimensional Ising model with coupling $\tilde{\lambda} = \frac{1}{2} \ln \coth \lambda$ [15]. It therefore has a second order phase transition, at $\lambda_c \sim .95$. For small β_v , one can integrate out the gauge field : this contributes, in the leading order, to only a renormalization of the coupling

$$\lambda \rightarrow \lambda_{eff} = \lambda + 4\beta_{\frac{1}{2}}^6 \quad (16)$$

where $\beta_{\frac{1}{2}}$ is given in eq. (12). Therefore, the transition will remain second order, at least to a point where the leading order approximation is valid. As β_v is increased, it becomes first order and joins the transition point on the

β_v - axis. We show the bulk phase diagram in Fig. 5. Apart from some details like the second order line etc., it is qualitatively the same as that in ref.[10]. For large β_v , the large λ region is smoothly connected to the small λ region. For, due to Eq. (9) the second term in action (15) is irrelevant here (any other configuration is strongly suppressed and can be treated in the dilute gas approximation). So the weak coupling limit is not changed by the addition of this term.

3.2 Study of the Finite Temperature Phase Transition

In order to study the true deconfinement phase transition which is unaffected by the bulk effects, we need to choose a value of $\lambda > \lambda_c$, so that the bulk transition can be avoided. For our simulations, we have used $\lambda = 1$. We checked that with this value of λ the plaquette variable is indeed smooth everywhere, indicating the lack of any bulk phase transition. The approximate location of the deconfinement transition is indicated by a steep rise in $\langle L_a \rangle$. We studied the deconfinement transition for lattices with $N_\tau = 2$ and 4. For finite size analysis, lattices with $N_\sigma = 8, 12$ and 16 were used for both N_τ .

For $N_\tau = 2$, the deconfinement transition was found to be at $\beta_v \sim 1.9$, while it was found to be at β_v around 2.3 for the $N_\tau = 4$ lattices. Both of these are close to the corresponding transition points for pure $SU(2)$ and far from the transition points for action (6) (see Sec. 2.2). We carried out simulations at a few β_v around the approximate transition point for each lattice size and then used multi-histogramming methods [16] to obtain the physical variables in the whole critical region. The details of the simulation are given in Appendix A. In Fig. 6 the behavior of $\langle L_a \rangle$ across the transition point, as obtained by the multi-histogramming extrapolation, is shown. $\langle L_a \rangle$ is seen to rise smoothly without any signs of a discontinuity in it. This is similar to its known behavior across the $SU(2)$ deconfinement transition. We also found that the $\langle L_a \rangle$ susceptibility did not show any peak at the transition point, again in agreement with the expectations from the $SU(2)$ theory.

A quantitative study of the order of the deconfinement transition is made difficult by the absence of an order parameter for this transition. The two physical variables that can be used are the energy density and specific heat. Extraction of these observables from lattice simulations is, however, difficult, as they are not simply related to objects directly measured in simulations. Since our purpose is only to show the existence of a deconfinement transition,

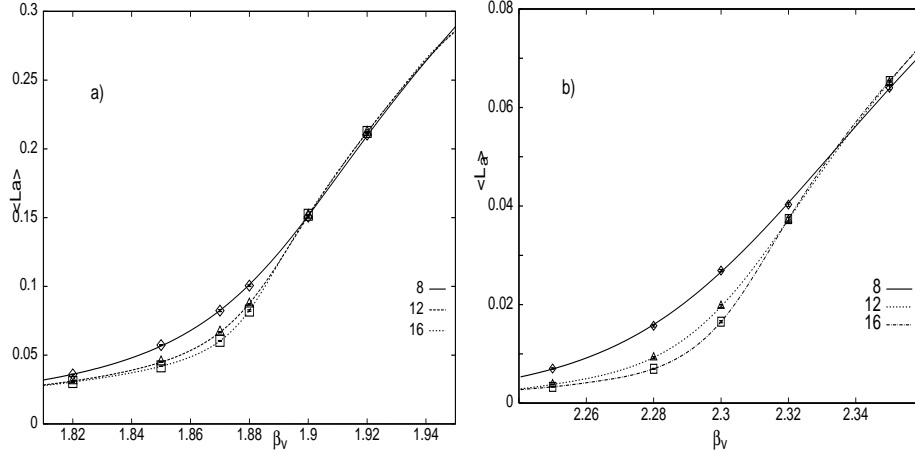


Figure 6: a) $\langle L_a \rangle$ across the deconfining point for $N_\tau = 2$ lattices with $N_\sigma = 8, 12, 16$. The points with error bars show the actual couplings where simulations were made. The curve is obtained by using multi-histogramming methods. b) Same for $N_\tau = 4$.

and not to make quantitative predictions about the transition, we use for these variables the approximate expressions (see Appendix B)

$$\varepsilon a^4 = 3\beta_v \langle P_\tau - P_\sigma \rangle, \quad (17)$$

$$C_v a^3 = 3N_\tau N_p \beta_v^2 \text{var}(P_\tau - P_\sigma), \quad (18)$$

where N_p is the number of spatial plaquettes, P_τ and P_σ are spatial and temporal plaquette variables respectively, and $\text{var}(x) = \langle x^2 \rangle - \langle x \rangle^2$. The energy density for $N_\tau = 2$ and 4 lattices is shown in Fig. 7. It is seen to rise significantly across the transition for both the N_τ values, justifying the identification of the transition as a deconfining one. The rise becomes steeper with increase in the spatial volume, indicating a true transition as opposed to a crossover.

The behavior of the specific heat for the $N_\tau = 2$ lattices is shown in Fig. 8. The position of the peak corresponds to the critical point. The peak height is seen to increase with the lattice size, and the peaks become sharper. Both these behaviors are expected for a deconfinement phase transition. While our expressions for specific heat, Eq. (18), are somewhat approximate to obtain an accurate critical exponent, it is interesting to note that a linear

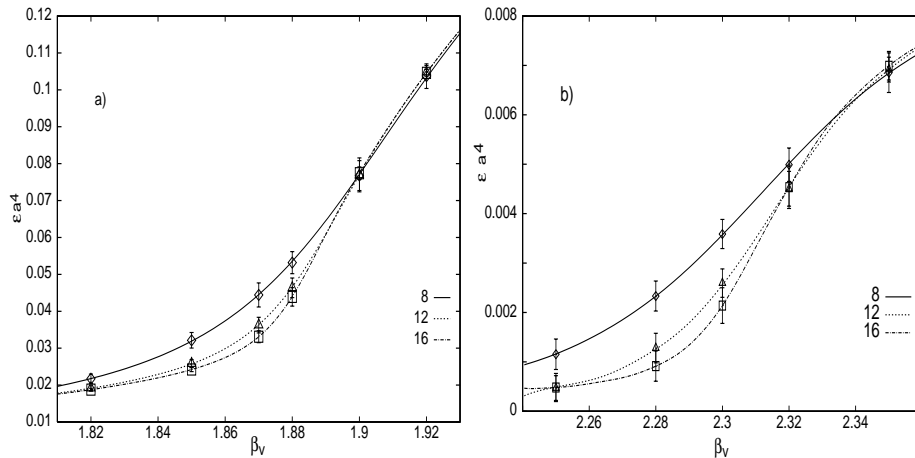


Figure 7: The energy density, Eq. (17), in the critical region of a) $N_\sigma^3 \times 2$ and b) $N_\sigma^3 \times 4$ lattices for $N_\sigma = 8, 12, 16$.

fit to the peak heights gives $\frac{\alpha}{\nu} = 0.13 \pm 0.04$, which is consistent with the three dimensional Ising model value $\frac{\alpha}{\nu} \simeq .17$. For the $N_\tau = 4$ lattices, the energy density being 16 times smaller in lattice units, the resultant specific heat curves were very noisy and inconclusive; a measurement of the exponent here is computationally very demanding and beyond our reach.

Thus the deconfinement transition for the monopole suppressed action of $SO(3)$ is very similar in nature to that for the $SU(2)$ Wilson action, although the former has no order parameter. A significant difference in the two, however, is the presence of negative $\langle L_a \rangle$ states in the $SO(3)$ theory. For the $SU(2)$ Wilson action, $\langle L_a \rangle$ approaches a unique positive value $\rightarrow 3$ as $\beta_f \rightarrow \infty$ in the high temperature phase. However, for $SO(3)$, $\langle L_a \rangle$ manifests itself in two states in the high temperature phase. One is like the high temperature state of $SU(2)$ but the other has a negative $\langle L_a \rangle$, which approaches -1 as $\beta_v \rightarrow \infty$. In ref. [3], it was proposed that the negative $\langle L_a \rangle$ state corresponds to a new bulk phase which is separated from the $\langle L_a \rangle \sim 0$ bulk phase by a bulk phase transition. From the behavior of the correlation functions, and the behavior of $\langle L_a \rangle$ in presence of a “magnetic” term hL_a in the action, it was concluded in ref. [5] that both the positive and negative $\langle L_a \rangle$ states correspond to the same physics. In the monopole-suppressed action, there is no bulk transition. However, we still find the negative $\langle L_a \rangle$ state, very similarly to the monopole unsuppressed action. In Fig. 9 we show

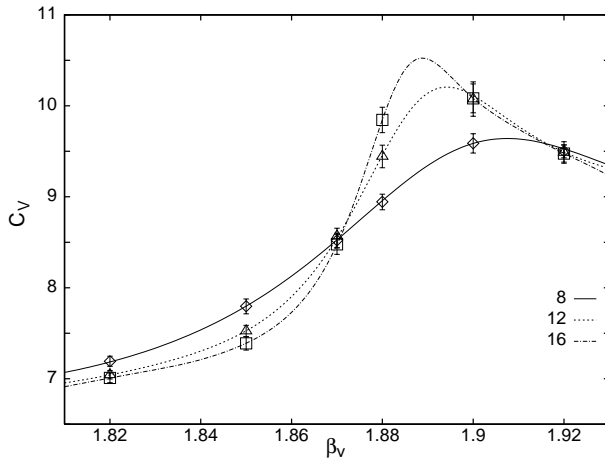


Figure 8: The specific heat density, Eq. (18), in the critical region of $N_\sigma^3 \times 2$ lattices for $N_\sigma = 8, 12, 16$.

the behavior of $\langle L_a \rangle$ for a large range of the coupling β_v , for both $\lambda = 0$ (the pure Villain action) and $\lambda = 1$ (the monopole suppressed case). Other than the shift in transition point, there is no essential difference between the two. Therefore the possibility advocated in ref. [3] of the negative $\langle L_a \rangle$ state being another bulk phase, separated by a bulk transition, is disfavored.

4 Summary and Discussion

We studied the $SO(3)$ lattice gauge theory in a Villain form numerically. Our main objective was to disentangle the effects of the bulk phase transition in this theory from those of the deconfinement phase transition in it, if any, and then to compare the latter with the $SU(2)$ theory which is expected to be in the same universality class. We attempted this by investigating the case of smaller $N_\tau = 2$ lattices and later by suppressing the Z_2 monopoles. Going to $N_\tau = 2$, the nature of the only transition observed was seen to change substantially compared to the earlier $N_\tau = 4-8$ studies. The transition point had a visibly large shift, and the order of the transition was found to change to second. However, the curious mix of bulk and finite temperature transitions, seen on lattices with higher N_τ , continued, as the behavior of the plaquette variables and that of $\langle L_a \rangle$, the adjoint Polyakov loop, were very similar.

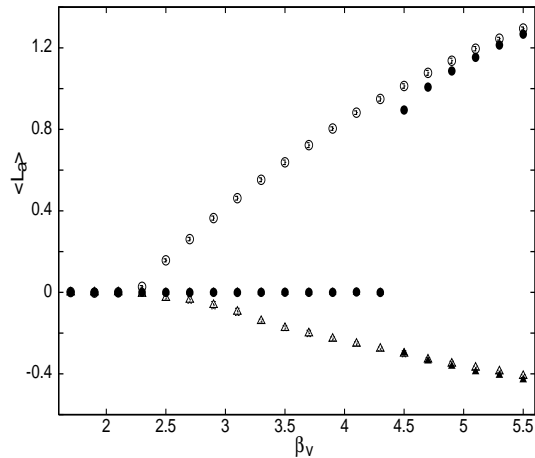


Figure 9: $\langle L_a \rangle$ for a range of couplings, showing the two different states in the high temperature phase. The filled circles and triangles correspond to the Villain action of Sec. 2 while the open circles and triangles correspond to the monopole suppressed action.

Determination of the critical exponents for their respective susceptibilities suggested a coincident bulk and deconfinement phase transition, similar to the higher N_τ studies but with a second order bulk transition. The scenario of bulk transition shielding the deconfinement transition, which was a plausible one for the higher N_τ lattices, is therefore disfavored, indicating the necessity of a more complicated scenario.

In order to get a clearer view of deconfinement in the $SO(3)$ theory, the bulk transition was evaded by adding a term in the action to suppress the topological objects driving the bulk transition. The resulting theory was found to have a deconfinement transition whose nature is very similar to the deconfinement transition in $SU(2)$. This is very interesting as the center symmetry, which plays a crucial role in the $SU(2)$ deconfinement transition, is trivial here, and the theory does not have any order parameter for its deconfinement transition. The location of the transition is also seen to be very different from that where the coincident bulk/deconfinement transition was seen for the Villain action without monopole suppression. It seems, therefore, that the bulk transition affects the deconfinement transition in a very subtle and nontrivial way, making it always coincide with itself. It would be very interesting to see two separate transitions for the original

$SO(3)$ theory without any monopole suppression on a big enough lattice, since these monopoles are mere lattice artifacts.

5 Acknowledgments

One of us (S.D.) would like to thank Profs. Frithjof Karsch, Sumit Das and Sourendu Gupta, and the other (R.V.G.) would like to thank Dr. Manu Mathur for stimulating discussions and suggestions.

A Details of Numerical Simulations

In this appendix we give details of the numerical simulations mentioned in the text. For all the simulations, we have used heat bath algorithms for both the gauge variables and the σ_p . An iteration consisted of updating all the link variables once, followed by an update of all σ_p . For the $N_\tau = 2$ measurements of Sec. 2.2, the transition point was approximately located for each lattice by looking for a phase coexistence. At this point a small run was made, and the spectral density method [11] was used to locate the susceptibility peak where a long simulation run was made. We used 1.6 million configurations for each lattice. Table 3 lists the couplings at which the long runs were made for different N_σ and the autocorrelation times for plaquette and L_a . For the extrapolations to nearby couplings using the spectral density method, the Jackknife estimate was used for both the extrapolated value and the error, using 20 blocks for the analysis. For the histograms of $16^3 \times 4$ and $24^3 \times 4$ lattices of this section, we produced 50000 configurations for each lattice, which was sufficient to clearly establish the peaks and nature of the histograms. The phase coexistence region was much broader for these lattices; we took $\beta_v = 4.45$, approximately at the middle of the region, for the longer runs. Due to the strong first order nature of the transition, tunnelings are not seen and we had to combine configurations from two runs to get the peaks.

For the simulations in Sec. 3.2, it was noticed that the plaquette variables have an extraordinarily large autocorrelation time. This can be reduced dramatically by implementing the energy-conserving steps corresponding to the center symmetry transformation (Eq. (8)). After every combined step of the previous section, we added another sweep where a fixed fraction (arbitrarily

Table 3: Details of the Monte Carlo simulations of Sec. 2.2.

N_σ	β_v	τ_P	τ_{L_a}
6	4.16	516.8	754.7
8	4.159	1010.4	1294.3
10	4.156	1738.5	1878.8
12	4.156	2245.7	2254.6
16	4.1552	2477.6	3896.5
24	4.1548	3155.8	4753.1

chosen to be one-fourth) of the total number of links, randomly chosen, are flipped along with all the plaquettes touching the link. An iteration consisted of the combination of this sweep with the combined heat bath step, and measurement was taken after every iteration. It was checked that for all the runs, the autocorrelation time was less than 100. For the $N_\tau = 2$ results of this section, from the rise in $\langle L_a \rangle$ the critical point was estimated to be $\lesssim 1.90$. We ran simulations at $\beta_v = 1.82, 1.85, 1.87, 1.88, 1.90$ and 1.92 , producing half million configurations at each coupling for each lattice. For the $N_\tau = 4$ case, the critical point was at ~ 2.30 . We produced one million configuration at $\beta_v = 2.30$, and half million configurations each at $\beta_v = 2.25, 2.28, 2.32$ and 2.35 . For interpolating to other values of β_v , each dataset was divided into very finely meshed histograms, and the multihistogramming techniques of ref. [16] was applied over the whole set. The central values and the errors quoted are Jackknife estimates, 20 blocks being used for the analysis in each case.

B The Energy Density and Specific Heat

The expressions for energy density and specific heat density, Eqs. (17) and (18), can be easily obtained using the methods of ref.[17]. We outline here the derivation of these results, emphasizing the approximations involved.

For finite temperature theory, it is necessary to take into account the asymmetry in the spatial and temporal directions by using two different

couplings. Writing

$$S = \beta_\sigma \sum_{\text{spatial } p} P_\sigma + \beta_\tau \sum_{\text{temporal } p} P_\tau, \quad (19)$$

the correct continuum limit is recovered by writing $\beta_\sigma = \frac{4}{g_\sigma^2} \frac{a_\tau}{a_\sigma}$ and $\beta_\tau = \frac{4}{g_\tau^2} \frac{a_\sigma}{a_\tau}$, where a_τ and a_σ are the temporal and spatial lattice spacings, respectively. The couplings g_σ and g_τ both equal the usual bare coupling g when the two lattice spacings are equal. In general, one can expand them perturbatively in g near the continuum limit [17]:

$$g_{\sigma,\tau}^{-2}(a_\sigma, a_\tau) = g^{-2}(a_\sigma) + c_{\sigma,\tau}(a_\sigma/a_\tau) + O(g^2).$$

Defining the inverse temperature $\beta = N_\tau a$, the energy density is given by

$$\begin{aligned} \varepsilon &= -\frac{1}{V} \frac{\partial}{\partial \beta} \ln Z|_V \\ &= -\frac{1}{N_\sigma^3 a_\sigma^3 N_\tau} \left\langle \frac{\partial S}{\partial a_\tau} \Big|_{a_\sigma} \right\rangle. \end{aligned} \quad (20)$$

From Eq. (19), one sees that evaluation of $\partial S / \partial a_\tau |_{a_\sigma}$ requires knowledge of the nonperturbative beta functions $\partial g_{\sigma,\tau}^{-2} / \partial a_\tau |_{a_\sigma}$, which, however, are not known for $SO(3)$ gauge theory. One can, therefore, use the perturbative expressions for the same, using the expansion in terms of g^{-2} given above. The perturbative beta functions are exactly similar to the $SU(2)$ case of ref. [17]. The contribution from this term is found to be small and does not affect the critical behavior. Ignoring this term, and putting $a_\sigma = a_\tau = a$ after taking the derivatives in Eq. (20), one gets the expression (17) for the energy density.

Similarly the specific heat at fixed volume is

$$\begin{aligned} C_v &= \frac{\partial \varepsilon}{\partial T} |_V = -\beta^2 \frac{\partial \varepsilon}{\partial \beta} \\ &= \frac{\beta^2}{N_\tau^2 V} \left\{ \left\langle \frac{\partial^2 S}{\partial a_\tau^2} \Big|_{a_\sigma} + \left(\frac{\partial S}{\partial a_\tau} \Big|_{a_\sigma} \right)^2 \right\rangle - \left\langle \frac{\partial S}{\partial a_\tau} \Big|_{a_\sigma} \right\rangle^2 \right\} \\ &= \frac{1}{V} \left\{ 2\beta N_p \langle P_\tau - P_\sigma \rangle + \beta^2 N_p^2 \text{var}(P_\tau - P_\sigma) \right\}, \end{aligned} \quad (21)$$

where P_σ is the plaquette variable on a symmetric lattice, and the coupling derivative terms have again been neglected. The first term in Eq. (21) is of same order as the neglected derivative terms, and should be omitted for consistency, giving us the expression (18). We have also checked that inclusion of the first term does not change the results in any significant way.

References

- [1] K. Wilson, Phys. Rev. D **10**, 2445 (1970).
- [2] A. V. Smilga, Ann. Phys. (N.Y.) **234**, 1 (1994).
- [3] S. Cheluvareja and H. S. Sharatchandra, hep-lat/9611001.
- [4] Saumen Datta and R. V. Gvai, in *Physics and Astrophysics of Quark-Gluon Plasma*, edited by B. Sinha *et al.* (Narosa Publishing House, New Delhi, 1998) p. 523.
- [5] Saumen Datta and R. V. Gvai, Phys. Rev. D **57**, 6618 (1998).
- [6] I. G. Halliday and A. Schwimmer, Phys. Lett. **101B**, 327 (1981).
- [7] G. Bhanot and M. Creutz, Phys. Rev. D **24**, 3212 (1994).
- [8] R. V. Gvai, M. Grady and M. Mathur, Nucl. Phys. **B423**, 123 (1994).
- [9] M. Mathur and R. V. Gvai, Nucl. Phys. **B448**, 399 (1995).
- [10] I. G. Halliday and A. Schwimmer, Phys. Lett. **102B**, 337 (1981).
- [11] A. M. Ferrenberg and R. H. Swendsen, Phys. Rev. Lett. **61**, 2635 (1988).
- [12] J. Lee and J. M. Kosterlitz, Phys. Rev. Lett. **65**, 137 (1990).
- [13] M. S. S. Challa, D. P. Landau and K. Binder, Phys. Rev. B **34**, 1841 (1986).
- [14] J. Fingberg *et al*, Phys. Lett. **B248**, 347 (1990).
- [15] R. Savit, Rev. Mod. Phys. **52**, 453 (1980).
- [16] A. M. Ferrenberg and R. H. Swendsen, Phys. Rev. Lett. **63**, 1195 (1989).
- [17] J. Engels, F. Karsch, H. Satz and I. Montvay, Nucl. Phys. **B205**, 545 (1982).